Constraints on friction coefficients by an inverse analysis of sand box thrust dips

Bertrand Maillot [a,*], Christophe Barnes [a], Jean-Marie Mengus [b], Jean-Marc Daniel [b]

[a] *Départment des Sciences de la Terre et de l'environment, CNRS-UMR 7072, Université de Cergy-Pontoise,*
5, mail Gay Lussac, Neuville-sur-Oise, 95031 Cergy-Pontoise, France
[b] *Division Géologie-Géochimie, Institut Français du Pétrole, Reuil-Malmaison, France*

Abstract

We measured the dips of thrusts forming in a uniform sand layer under horizontal shortening by a rigid emerging ramp in conditions of full erosion. Various ramp dips and four types of ramp material were used throughout the 12 experiments. In three experiments, the ramp was short-cut by a less steep thrust forming a spontaneous ramp in the sand. The forward modelling proposed to predict these observations involves (i) computing the total dissipation in the structure by using global force equilibrium and a parameterised kinematic framework including the possibility of shortcut development, and (ii) minimising the total dissipation of mechanical work with respect to the kinematic parameters (i.e., the thrust dips), for which two analytic solutions are found. The inverse problem involves computing probability densities over the parametric space of friction coefficients, including the internal friction angle of the sand, and friction angles of the four materials used on the rigid ramps. Practically, this involves computing a misfit (using the L2 norm) between the observed and predicted thrust dips for every possible value of the friction angles. The resulting probability density provides all the quantitative information that can be retrieved from the experiments in the light of our forward modelling. Ramp friction angles exhibit sharp probability changes at values that trigger the occurrence of shortcuts, thus yielding non-trivial bounds on the ramp friction values that are directly related to the observations of ramp and back thrust geometry. Also, the probability distribution of the internal sand friction, and those of the ramp frictions, is in good agreement with independent measurements. This approach is designed to be applicable to field studies of brittle deformation where geometries are observed and rheological parameters are sought.
© 2006 Elsevier Ltd. All rights reserved.

Keywords: Analogue modelling; Friction coefficient; Thrust dip; Inverse problem; Fault-bend fold

1. Introduction

Fold-and-thrust belts are classically characterized by the shortening of sedimentary layers above horizontal décollement layers that lie at decreasing depths towards the exterior of the orogenic belt (Rich, 1934). These various décollements join by reverse faulting across more competent layers, forming a series of ramps. Generic kinematic models of this flat−ramp−flat geometry (e.g., Suppe, 1983) have proven useful in the construction of balanced cross-sections, and in the interpretation of microstructures formed due to large scale folding associated with thrust ramps (e.g., Grelaud et al., 2000). However, these models are less helpful in relating field observations to rheological parameters because they make no reference to force balance. The use of analogue models with well known rheological parameters gives some insight into these problems (e.g., Merle and Abidi, 1995; Bonini et al., 2000; Persson, 2001); although conclusions often remain qualitative because forces are not measured or modelled. Numerical simulations, which solve the full boundary valued problem, offer complementary insights (e.g., Erickson and Jamison, 1995; Erickson et al., 2001), although they often face problems related to

* Corresponding author. Tel.: +33 134257359; fax: +33 134257350.
 E-mail address: Bertrand.maillot@u-cergy.fr (B. Maillot).

strain localisation or the effects of sharp boundary conditions. This makes it difficult to perform detailed comparisons of their outputs with analogue models (e.g., see Buiter et al., 2006; Schreurs et al., 2006, and references therein). Thus, analogue and numerical models are experimental tools used to help us better understand the deformation mechanisms and tectonic structures. Ideally, each should be tested against analytical solutions when possible. This allows analogue experiments to get closer to a full quantitative analysis, while numerical solutions can be tested for convergence. The present paper is our third contribution in this line of research.

Using a kinematic model of fault-bend folding (Suppe, 1983) as a starting point and inspired by Merchant's (1944) approach of the mechanics of metal cutting, Maillot and Leroy (2003) have proposed a model that optimizes the dissipation of mechanical work with respect to the dip of the transition zone between the hanging walls of the lower flat and ramp, which may appear as a reverse fault or as a ductile hinge. They showed in particular that the dip is less than that which is usually assumed in kinematic models, leading to a thickening of the hanging wall above the ramp. This prediction has been verified using sand box experiments (Maillot and Koyi, 2006). In the present paper we apply our theoretical approach to the horizontal shortening of a single sand layer over a rigid ramp in a steady-state regime involving full erosion of any built-up surface relief. This setup is analogous to the shortening of sedimentary layers cut by pre-existing normal faults due to an older extensional phase. Numerous examples can be found in the literature (e.g., Roure and Colletta, 1996), most notably in the Colombian and Venezuelan Andes, and the French sub-alpine massifs (e.g., see Colletta, 2005). Here, we present a new analytical solution which generalises Anderson's prediction of dips of conjugate reverse faults for the case of faults with different friction angles. In an attempt to illustrate how such theoretical predictions can be used to analyze field data of thrust dips, we treat our sand box experiments as if they were field observations: thrusts can be identified and their dips can be measured, but their rheological parameters remain unknown. We propose to use the inverse problem theory (Tarantola, 1987) to gain quantitative information on these parameters.

The contents of the paper are as follows. In Section 2, we present a series of 12 experiments in which a uniform sand layer is compressed horizontally over a rigid ramp with conditions of full erosion. Six ramp dips (from 19° to 66°) and four types of frictional surfaces were used. The sand responds by forming a series of thrusts that allow it to slide upward over the imposed ramp. In three experiments, the imposed ramp was shortcut by a less steep spontaneous ramp in the sand. For most experiments the thrust dips follow a Gaussian distribution, as indicated by a χ^2 test. The direct problem is presented in Section 3. Assuming a purely frictional behaviour for the sand, a forward model is developed in which (i) the total dissipation in the structure is computed by combining the known kinematics, parameterised using the ramp and thrust dips, with a global force equilibrium of rigid blocks, and (ii) the total dissipation is minimised with respect to the thrust

dips (Maillot and Leroy, 2003). Finally, the inverse problem presented in Section 4 involves computing probability densities over the parametric space of the friction coefficients (a five dimensional space defined by the internal friction angle of the sand, and the friction angles of the four materials used on the rigid ramps). Practically, this involves computing a misfit (using the L2 norm, in accordance with the Gaussian character of the data) between the observed and predicted thrust dips for every possible value of the friction angles. The resulting probability distributions show for each friction angle the range of values compatible with the experiments. They prove to be in agreement with independent friction measurements. The results reproduce very clearly the phenomenon of shortcuts as well as the dependency between ramp and thrust friction values and provide probabilistic upper or lower bounds on the friction coefficients of the various ramps.

2. Description of the experiments

2.1. Experimental setup

In the 12 experiments, a layer of dry sand was compressed by the horizontal movement of a rigid ramp (Fig. 1). All surface relief created was eroded using a scraping board following every 10 mm of shortening. Various ramps were used with dips ranging from 19° to 66° (Table 1, column 4), and surfaces made of four types of materials (groups A, B, C, and D in Table 1, column 3). The sand layer width was $w = 50$ cm, the length was $l = 20$ cm (experiments 1–6), or 35 cm (experiments 7–12), and the thickness e_i is given in Table 1, column 2. The width of the box (1 m) allowed us to let the sand fall freely to the sides, without lateral side walls. The shortening was applied until thrusts emerged close to the back wall. The total shortening achieved ranges between 2 and 14 cm. In all experiments, sand was slowly poured from a height of about 20 cm, by the same person. Experiment 3 is a repetition of experiment 2, but the sand was statically compacted by firmly pressing a flat rigid board on the sand surface before starting the shortening. No substantial differences were noticed in the dip measurements of these two experiments (columns 6 and 7 of Table 1). Although it represents substantial amount of laboratory work, 12 experiments represent a rather small sample from the point of view of inverse problem theory. In such a case, it is preferable to let the parameters vary simultaneously (ramp dip and ramp friction) rather than one by one: the sampling of the parametric space is therefore made more efficient.

2.2. Properties of the analogue materials

The Nemours sand used in all experiments is a natural sand sieved between 80 and 120 μm, with a sharp peak at 100 μm. Its density is 1.53 ± 0.02 and its failure envelope is $\tau = (0.615 \pm 0.03)\sigma_n + 80 \pm 22$ Pa which corresponds to a friction angle ranging between 30.3° and 32.8°. The friction of this sand against the ramps of type B (P150 sand paper) follows $\tau = (0.691 \pm 0.004)\sigma_n - 20 \pm 6$ Pa (friction angle
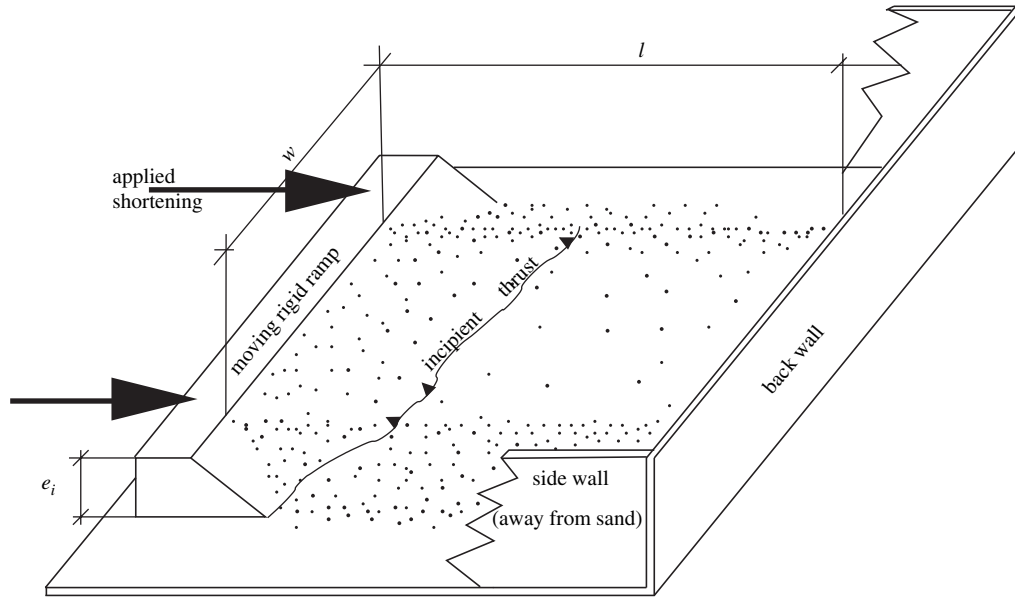
Fig. 1. Schematic diagram of the sand box. Note that the side walls are not in contact with the sand, which spreads freely in the box ($w = 50$ cm, and the box is 1 m wide). The side walls serve only to guide the scraping board when eroding any relief above the height e_i of the rigid ramp.

between 34.5° and 34.8°). For ramps of type D (fiber glass sheet), $\tau = (0.426 \pm 0.005)\sigma_n + 51 \pm 11$ Pa (friction angle between 22.8° and 23.3°). All these frictional properties were determined previously by Maillot and Koyi (2006). Friction values of the sand against the ramp materials used in groups A and C have not been measured. However, the PVC and varnished wood surface used in group A is smooth and hard and is expected to have a low friction value, while the plaster coated and sanded raw wood used in group C should have a friction value lying between those of groups B (sand paper) and D (smooth and soft fiber glass sheet). Thus the ramp friction values may be reliably placed in increasing order: A < D ($\mu = 0.426 \pm 0.005$) < C < B ($\mu = 0.691 \pm 0.004$). The bottom of the box was covered with a fiber glass sheet with the same friction as ramps of type D given above.

2.3. Measurement and statistical description of the experimental results

The dips of the ramp (φ) and thrusts (θ) were measured by hand picking the active faults from scanner images. Scanner cross-sections were taken ever 3 cm along strike at the end of each experiment with a definition of about 1 mm. Active faults were determined by the offset they produce in the surface topography since the last erosion event (i.e., last 10 mm of horizontal shortening). Curved faults were sampled using short straight segments, with each segment constituting one independent measurement. These raw data were then weighted proportionally to segment length in order to give more importance to a planar thrust crossing all the sand layers compared to a small segment. In general, along dip and along strike

Table 1
List of experiments. Columns 2–4 give the thickness of the sand layer (e_i, column 2) that was shortened by an imposed right ramp dipping at φ' (column 4) and made of material A, B, C, or D (column 3, see Section 2 for an explanation)

Experiment number	Thickness e_i (mm)	Ramp material	Ramp dip φ' (°)	Kinematic case	$\overline{\varphi} \pm \sigma_\varphi$ (°)	$\overline{\theta} \pm \sigma_\theta$ (°)	Number of samples	Q (χ^2) (%)
1	28	A	30	1	30 ± 0.25	37.2 ± 8.2	57	9.6
2	41	A	49	1	49 ± 0.25	33.9 ± 3.3	20	13
3	41	A	49	1	49 ± 0.25	34.1 ± 4.2	65	62
4	55	A	66	1	66 ± 0.25	29.5 ± 4.4	58	15
5	103	B	66	3	40 ± 6	31.8 ± 3.9	22	70
6	92	B	50	3	48 ± 1	32 ± 3.9	52	27
7	93	C	34	1	34 ± 1	28.1 ± 5	214	99
8	78	C	19	1	19 ± 1	25.5 ± 6	23	99
9	94	C	51	1–3	43 ± 8.3	24.4 ± 4.8	65	68
10	91	D	27	1	27 ± 0.25	32.9 ± 6.9	127	1.8
11	91	D	35	1	35 ± 1	37 ± 9	159	26
12	91	D	49	1	49 ± 1	33.6 ± 8.5	209	1.7

Column 5 gives the observed kinematic case (Fig. 4). Columns 6 and 7 give the mean observed ramp dip ($\overline{\varphi}$) and thrust dip ($\overline{\theta}$), with their respective standard deviations (σ_φ and σ_θ). Column 8 is the number of independent measurements of θ. Column 9 is the probability that the distribution of measured values of θ is Gaussian (according to a χ^2 test). Only the distributions of experiments 10 and 12 appear non-Gaussian.

variations in the thrust dip, due to curvature and the anastomosing character of the faults are well above the definition of the scanner images. We now describe successively the measurements of ramp dips and of thrust dips. Since only a single ramp is active in each experiment, along which many thrusts are created and uplifted, the statistical analysis can only be performed on the thrust dips, not on the ramp dips. The ramp dips φ were in general equal to the imposed, rigid, ones (φ') and could be determined with a high level of precision. Error bars of $0.25°$ were added to these imposed dips in order to avoid infinite misfits during the inversion procedure (the $1°$ value in experiments 7, 11, and 12 allows for the actual irregularity of the imposed ramp). When different from the imposed ramp, the spontaneous ramp may exhibit large standard deviations σ_φ around its mean dip $\overline{\varphi}$ (experiments 5 and 9) and this is partly due to the small number of independent measurements. For experiment 9, the large standard deviation ($8.3°$) is due to large variations along strike, further discussed in the next paragraph. We now describe the measurements of the thrust dips θ. The numbers of independent measurements n are indicated in Table 1, column 8 ("number of samples"): they range from 20 to 214 with an average of 90 measurements per experiment. Histograms of the thrust dips in $2°$ bins for each experiment are shown in Fig. 2. The resulting mean value $\overline{\theta}$ and standard deviation σ_θ of the thrust dips (Table 1, column 7) were used to compare our measured dip distributions with a Gaussian distribution

$$P(\theta) = e^{-\frac{1}{2}\left(\frac{\theta - \overline{\theta}}{\sigma_\theta}\right)^2}. \tag{1}$$

Like Gaussian distributions, most histograms exhibit a single mode with a symmetric distribution, although the amplitude of the mode is always larger than that of a Gaussian distribution (experiments 3, 4, 5, 6, and 7). Some experiments exhibit asymmetry (experiments 2, 9, and 12) or are bi-modal (experiment 1, and perhaps 8, 10, and 11). Qualitatively, it is easy to see from Fig. 2 that experiments 3, 4, 5, 6, 7, and 11 seem reasonably Gaussian, while the others (1, 2, 8, 9, 10, and 12) seem either bi-modal, or asymmetric. A useful quantitative comparison is the χ^2 test which we performed as follows. First, the range of dip values $[0°, 90°]$ is divided into 10 bins at values t_i ($i = 0, \dots 10$), such that they have equal theoretical probabilities:

$$\int_{t_i}^{t_{i+1}} P(\theta)\, d\theta = f_{th} = 0.1, \quad \forall\ i = 0, \dots 9, \tag{2}$$

where $t_0 = -\infty$ and $t_{10} = +\infty$, and such that the sum of probabilities of all the bins is 1. For experiments 2, 5, and 8 with
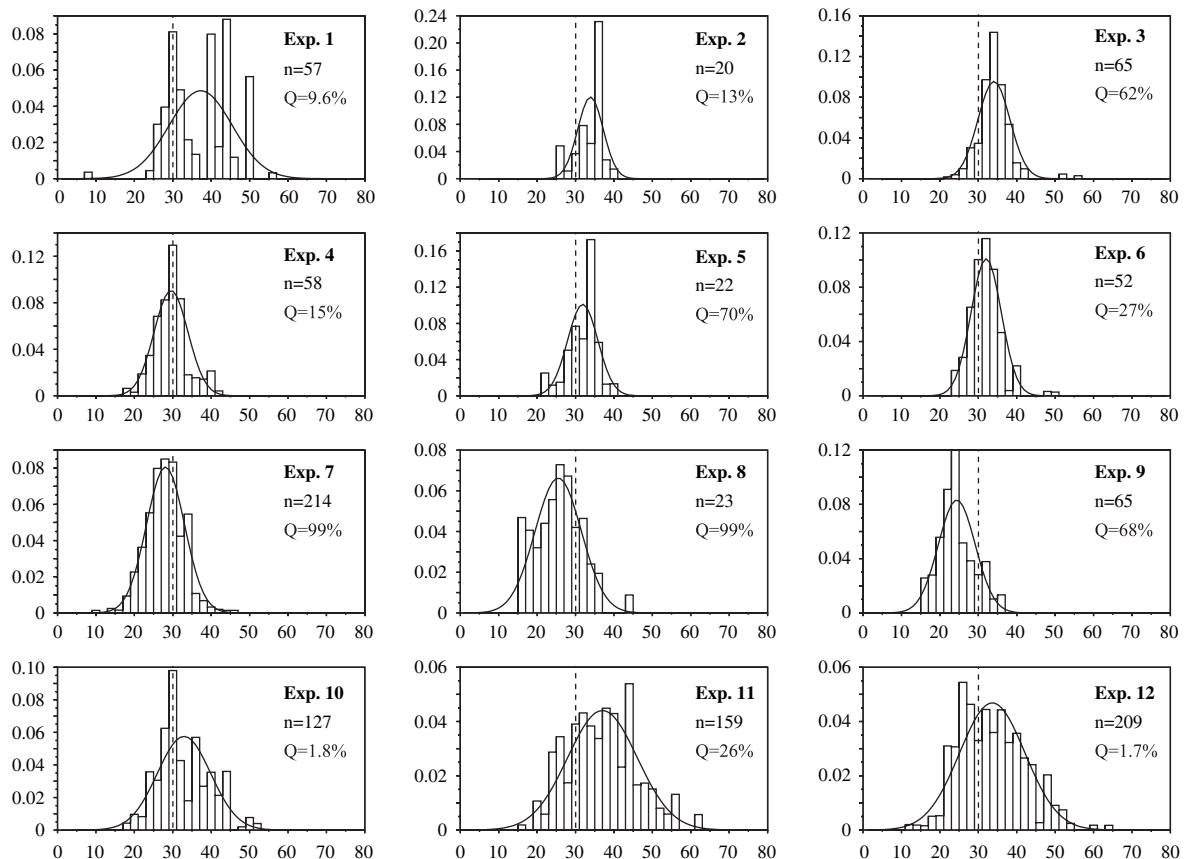

Fig. 2. Histograms of thrust dips θ for each experiment. The solid curves are the corresponding theoretical Gaussian distributions. To help comparison, a stippled line is drawn at $30°$ in all graphs. n is the number of samples, or independent measurements, of θ. Q is the probability for the histogram to follow a Gaussian distribution according to the χ^2 test.

less than 50 measurements, five bins were used instead of 10 (in which case, $f_{th} = 0.2$, and $i = 0, \ldots 4$ in Eq. (2)). Observed frequencies of measurements $f_{obs}(i) = n(i)/n$ were than calculated from the tenth (or fifth) t_i ($n(i)$ is the number of dips measured between t_{i-1} and t_i). Then, we use χ^2 as an indicator of dispersion of the observed frequencies with respect to the theoretical ones:

$$\chi^2 = n \sum_{i=1}^{9} \left(\frac{f_{obs}(i) - f_{th}}{f_{th}} \right)^2. \tag{3}$$

Finally, the probability that the observed distribution is a Gaussian distribution is given by the integral from χ^2 to $+\infty$ of the χ^2 distribution function, that is noted $Q(\chi^2)$ and given in percent in Table 1, column 9. For a perfect Gaussian distribution, $\chi^2 = 0$ and $Q = 100\%$. Typically, a value of Q below 3% or 5% indicates a distribution that cannot be considered to be Gaussian. Surprisingly, experiment 1 gives a better test than experiment 12. Also, experiments 10 and 12 fail the test whilst experiment 8 succeeds almost perfectly! The reason is that the test depends strongly on the total number n of independent measurements used in Eq. (3). With small amounts of data, the test suggests a Gaussian distribution even though the histogram does not look Gaussian. In contrast, the distribution can look reasonably Gaussian and have a negative test (experiment 10) because there are a lot of data available so that each departure from a Gaussian distribution is very informative and constraining. We conclude that the Gaussian statistical model is acceptable for our data, given the available amounts of independent measurements. The choice of a Gaussian model for the data allows us to choose with confidence the L2 norm in the definition of the misfit (19) during the inversion procedure.

2.4. Qualitative description of the experimental results

The compression resulted in the development of thrusts in the sand layer (Figs. 3a, and 4, top), and possibly of a spontaneous ramp if the imposed one was not favourably oriented for slip (see illustration in Fig. 3b; a list of such experiments in Table 1, column 5; and the idealised kinematics in Fig. 4, bottom). The mean thrust dip $\overline{\theta}$ reaches a maximum for ramp dips $\varphi \approx 30°$, and decreases for higher or lower ramp dips, regardless of the type of ramp material used. Conversely, for a fixed ramp dip, $\overline{\theta}$ decreases systematically with an increase in ramp friction (compare experiments 3, 12, and 9). However, $\overline{\theta}$ exhibits a relatively narrow range throughout the experiments (24–37°) compared to the range of imposed ramp dips
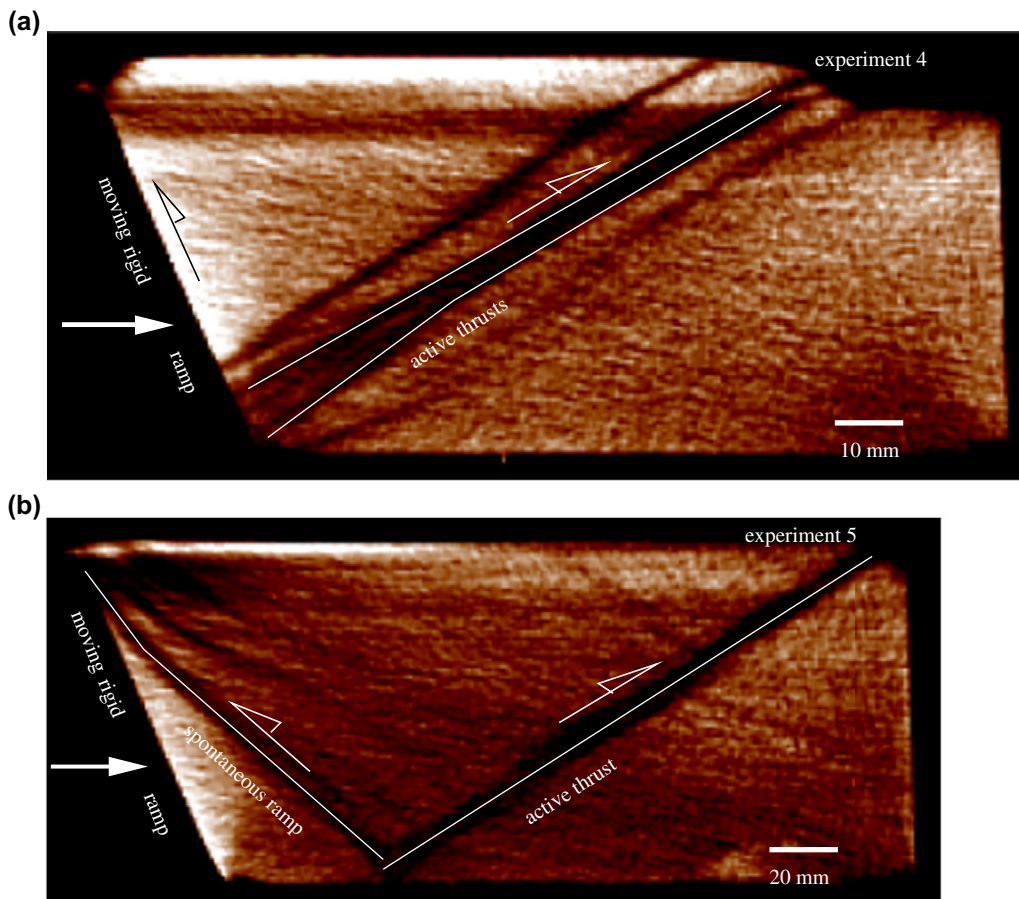

Fig. 3. Scanner images of two typical experiments where the movement of the rigid ramp creates thrusts in the sand (a) and may be shortcut by the creation of a spontaneous ramp (b). (a) and (b) are, respectively, modelled as cases 1 and 3 in the theoretical geometries of Fig. 4.
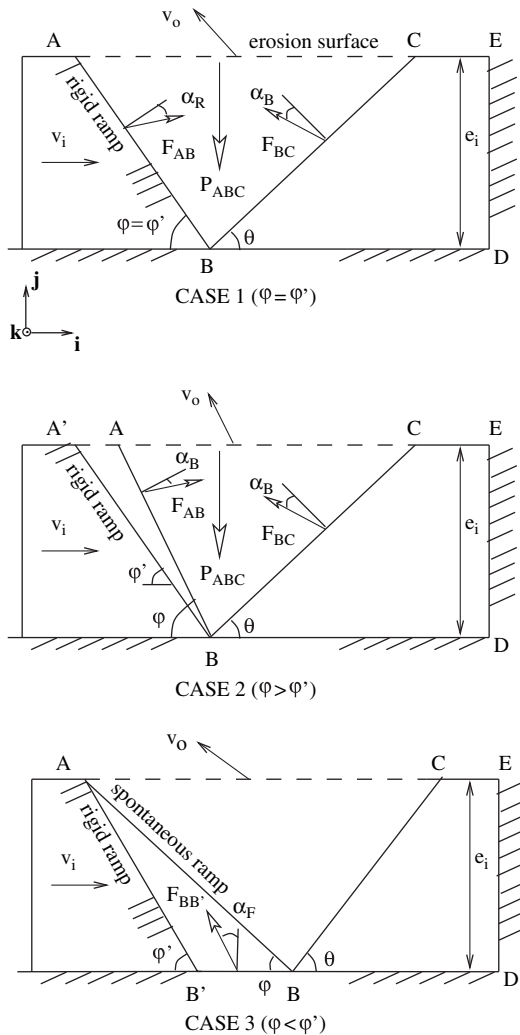
Fig. 4. The model problem described in case 1 (top) involves the horizontal movement of the rigid ramp (AB) with dip φ' at velocity v_i, creating thrusts (BC) with dip θ in a homogeneous sand layer (AEDB) of thickness e_i. The ramp hanging wall slides at velocity v_o relative to the ramp and is fully eroded at surface (AC). The total forces acting on the ramp hanging wall are its weight $\mathbf{P}_{ABC}$, equilibrated by the ramp reaction $\mathbf{F}_{AB}$, and the thrust reaction $\mathbf{F}_{BC}$. α_F, α_B, α_R denote the friction angles of the flat, the thrust, and the ramp, respectively. In case 2 (middle), a spontaneous ramp has formed in the sand, with a higher dip ($\varphi > \varphi'$). In case 3 (bottom) the spontaneous ramp has a lower dip ($\varphi < \varphi'$). In case 3, additional dissipation along the flat (BB') must be accounted for.

(19–66°) thus suggesting that the thrust dip is relatively insensitive to the dip of the imposed ramp. More interesting is the occurrence (experiments 5, 6, and 9), or absence, of shortcuts. This qualitatively different behaviour, and the very fact that it did not occur in nine experiments despite the wide range of ramp dips tested, brings a strong constraint on the friction parameters of the sand relative to those of the ramps that will be highlighted and quantified by the inversion process. Finally, the sand layer thickness (Table 1, column 2) has apparently no substantial effect on the experimental results, and is given here for completeness of information. Also, because of the full erosion, a steady state is reached very quickly and the total amount of shortening applied has very little effect on the thrust

dips. Thus, variations in sand layer dimensions and in the total shortening applied are disregarded in the following analysis of the ramp and thrust dips. Pre-compaction (experiment 3) and dilatancy along thrusts are also disregarded. Similarly, along strike, and along dip variations in the fault surfaces are not studied in detail, but are all integrated into the standard deviations σ_φ and σ_θ. The only detail useful to note concerns along strike variations in experiment 9: the sand was sliding along the imposed ramp on one side of the box, but created a spontaneous ramp on the other side. Since we did not reject any experiment, this one was measured like all others, and the resulting very large standard deviation of the ramp dip (8.3°) automatically decreases its influence on the results of the inversion, as one should expect. This lack of precise information from experiment 9 probably has its origin in the relatively large discrepancy between inverted and independently measured friction angles for the ramps of type C, as further discussed in the inversion section.

The goal of the present work was to answer the following question: What can be said about the friction coefficients of the analogue materials given the series of 12 experiments presented above? More specifically, we would like to be able to draw quantitative conclusions concerning the friction parameters of the sand onto itself and on the four ramp materials (A, B, C, and D). The answer can be found by inverting together all the dip data (ramp and thrusts) with respect to the frictional parameters as shown in the inversion section. However, the direct problem must first be solved, and this is treated in the next section.

3. The direct problem

The question specific to the experiments presented here is: What are the dips of the two reverse faults (ramp and thrust) appearing in the sand as functions of the dip of the imposed ramp and of the friction parameters? The answer is provided by the forward model presented below following Maillot and Leroy (2003), and validated experimentally by Maillot and Koyi (2006).

The solution involves finding the dips that minimise the total dissipation of mechanical work in the structure. The work is defined as the product of the shear force by the slip rate along the active faults. We have defined three kinematic scenarios for the active faults. Of these three scenarios, the optimal one is the one that yields the smallest total dissipation, and the solution to the direct problem is given by the optimal thrust dips for the optimal scenario. These scenarios are illustrated in Fig. 4 as case 1 (top), where the sand slides on the imposed rigid ramp at velocity v_0, case 2 (middle) where the sand creates a steeper spontaneous ramp, and case 3 (bottom) where the spontaneous ramp has a lesser dip than the imposed one. Column 5 of Table 1 shows that all experiments follow the case 1, except experiments 5 and 6 which follow case 3, and experiment 9 which, we recall, varies from 1 to 3 along strike. No experiment corresponds to case 2 which is used here for completeness of the solution of the direct problem. Case 2 has of course been observed in other analogue experiments

with very low ramp dips (e.g., Persson, 2001). In all cases we assume that the dissipation of energy occurs only by friction along the active ramp (AB) and the thrust (BC), and neglect the dissipation due to diffuse deformation in the sand. Note that case 3 implies additional dissipation by friction along the flat segment (BB'). Let us now develop the theory for each case.

3.1. Case 1

We assume that the flow of sand is stationary and isochoric, hence

$$v_o \sin(\theta + \varphi) = v_i \sin \theta, \tag{4}$$

obtained by stating that entry (v_i) and exit (v_o) velocities must have the same component perpendicular to the thrust. This choice of simple kinematics implies that we neglect dilatancy. θ is the dip of the thrust (BC), and φ is the dip of the thrust (AB) which for case 1 coincides with the imposed ramp dip $\varphi' = \varphi$. As the material flux through the thrust (BC) is constant ($v_i e_i = v_o e_o$), it provides the following thickening or thinning relation

$$e_o = e_i \frac{\sin(\theta + \varphi)}{\sin \theta}. \tag{5}$$

The dissipation along each thrust is defined as the product of the velocity jump across the thrust by the shear force it sustains. Thus the dissipations along the ramp (AB) and the thrust (BC) are, respectively,

$$D_{AB} = T_{AB} v_i \frac{\sin \theta}{\sin(\theta + \varphi)}$$

$$D_{BC} = T_{BC} v_i \frac{\sin \varphi}{\sin(\theta + \varphi)}, \tag{6}$$

where

$$T_{AB} = \tan \alpha_R N_{AB}$$

$$T_{BC} = \tan \alpha_B N_{BC} \tag{7}$$

are the mean shear forces acting, respectively, on the ramp (AB) and thrust (BC), N_{AB} and N_{BC} are the mean forces normal to these thrusts, and α_R and α_B, the respective friction angles. By adopting these Mohr–Coulomb relations we consider a purely frictional behaviour of our sand and neglect the small amounts of cohesion, strain-softening and again, dilatancy, that are likely to be present (e.g. Lohrmann et al., 2003). The forces T_{AB} and T_{BC} are determined by invoking the global equilibrium of the hanging wall (ABC):

$$\mathbf{F}_{AB} + \mathbf{F}_{BC} + \mathbf{P}_{ABC} = 0. \tag{8}$$

The weight $\mathbf{P}_{ABC}$ is easily determined from Fig. 4:

$$\mathbf{P}_{ABC} = -\frac{1}{2}\rho g e_i^2 \frac{\sin(\theta + \varphi)}{\sin \theta \sin \varphi}\mathbf{j}. \tag{9}$$

Projecting the equilibrium Eq. (8) along axes ($\mathbf{i}$, $\mathbf{j}$) (Fig. 4) and writing the mean forces $\mathbf{F}_{AB}$ and $\mathbf{F}_{BC}$ in terms only of their shear components with the help of Eq. (7) yields two equations with solutions

$$T_{AB} = \frac{1}{2}\rho g e_i^2 \frac{\sin(\theta + \varphi)\sin(\theta + \alpha_B)\sin \alpha_R}{\sin(\theta + \varphi + \alpha_R + \alpha_B)\sin \theta \sin \varphi}$$

$$T_{BC} = \frac{1}{2}\rho g e_i^2 \frac{\sin(\theta + \varphi)\sin(\theta + \alpha_R)\sin \alpha_B}{\sin(\theta + \varphi + \alpha_R + \alpha_B)\sin \theta \sin \varphi}. \tag{10}$$

Eqs. (10) and (6) complete the calculation of the total dissipation

$$D_T = D_{AB} + D_{BC}. \tag{11}$$

The optimal thrust dip θ_{opt} with respect to the total dissipation verifies

$$\frac{\partial D_T}{\partial \theta} = \sin^2 \theta_{opt} - \sin\left(2\theta_{opt} + \varphi + \alpha_R + \alpha_B\right)\frac{\sin \alpha_B}{\sin \alpha_R}\sin \varphi = 0. \tag{12}$$

The solution is

$$\theta_{opt} = \text{arctg}\left(\frac{A \cos \beta + \sqrt{A^2 + A \sin \beta}}{1 + A \sin \beta}\right), \tag{13}$$

$$A = \frac{\sin \alpha_B}{\sin \alpha_R}\sin \varphi, \quad \text{and} \quad \beta = \varphi + \alpha_R + \alpha_B. \tag{14}$$

This solution is illustrated in Fig. 5 for a reference parameter set $\alpha_R = 20°$, $\alpha_B = 30°$, $\varphi = 25°$, each curve showing the effect on θ_{opt} of one of the parameters (α_R, α_B, φ). Clearly, and maybe counter-intuitively, the friction α_R along the imposed ramp is the most important parameter controlling the thrust
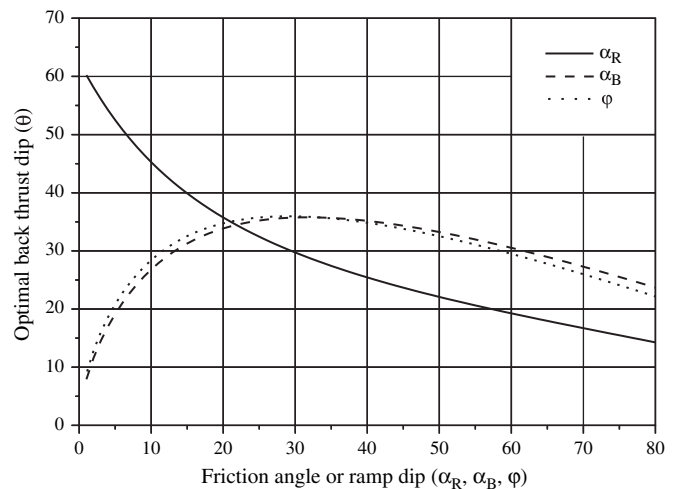
Fig. 5. Optimal thrust dip (θ_{opt}) in case 1 of Fig. 4 (analytic solution (13)), for $\alpha_R = 20°$, $\alpha_B = 30°$, $\varphi = 25°$, except for the parameter selected to vary as indicated in the inset.

dip θ_{opt}. It is in particular more important than the friction α_{B} on the thrust itself.

3.2. Case 2

In case 2 (Fig. 4, middle), all the dissipation occurs again along the spontaneous ramp (AB) and thrust (BC). No additional dissipation is considered in the spontaneous foot wall (ABA′) since the imposed ramp (A′B) is not active. We must now optimise the total dissipation (11) with respect to both thrust dips θ_{opt} and φ_{opt} by solving Eq. (12) together with

$$\frac{\partial D_{\text{T}}}{\partial \varphi} = \sin^2 \varphi_{\text{opt}} - \sin\left(\theta_{\text{opt}} + 2\varphi_{\text{opt}} + \alpha_{\text{R}} + \alpha_{\text{B}}\right)\frac{\sin \alpha_{\text{R}}}{\sin \alpha_{\text{B}}}\sin \theta_{\text{opt}}$$
$$= 0, \tag{15}$$

and setting $\alpha_{\text{R}} = \alpha_{\text{B}}$ since both thrusts occur within the sand. The solution is

$$\theta_{\text{opt}} = \varphi_{\text{opt}} = \frac{\pi}{4} - \frac{\alpha_{\text{B}}}{2}, \tag{16}$$

with the additional condition that $\varphi_{\text{opt}} > \varphi'$, the dip of the imposed ramp (A′B). If $\varphi_{\text{opt}} < \varphi'$, case 3 must be considered.

The solution (16) deserves some comments, because it coincides with the dips of conjugate reverse faults that would be obtained both from a Mohr circle construction, and by Anderson's theory of faulting (e.g., Turcotte and Schubert, 1982, p. 354). Anderson's prediction is similar to the one presented here in that it is the result of a minimisation. The difference is that Anderson assumes a known stress distribution whereas we start from a known kinematic framework, which is directly linked to field observables and from which we can then deduce mean forces by invoking global equilibrium. In fact, from the mechanical point of view of limit analysis, these approaches to the solution (16) are complementary. Anderson's approach yields a lower bound to the tectonic force necessary to create conjugate faults, because the calculations are done in a medium that is not *yet* fractured. Our kinematic approach, in contrast, yields an upper bound, because the tectonic force is calculated in a medium where the fractures are *already* active. The coincidence of the two bounds proves that Eq. (16) is the exact solution to the problem of case 2.

3.3. Case 3

There are three sources of dissipation in the case 3 of Fig. 4 (bottom): the spontaneous ramp (AB), the thrust (BC) and the flat thrust (B′B). Dissipations along (AB) and (BC) are calculated as in case 2. Dissipation along (B′B)

$$D_{\text{B′B}} = T_{\text{B′B}} v_{\text{i}} \tag{17}$$

requires us to calculate the equilibrium of the block (ABB′) to determine the mean shear force $T_{\text{B′B}}$, again related to the mean normal force $N_{\text{B′B}}$ by the Mohr–Coulomb relation $T_{\text{B′B}} = \tan \alpha_{\text{F}} N_{\text{B′B}}$. Since there is no slip along the rigid

ramp AB′, we have $0 < T_{\text{AB′}} < \tan \alpha_{\text{R}} N_{\text{AB′}}$. We have set $T_{\text{AB′}} = 0.9 \tan \alpha_{\text{R}} N_{\text{AB′}}$, and checked that $N_{\text{AB′}} > 0$, i.e., the block *ABB′* is not lifted upward. No analytic solution was found, and the optimal thrust dips must therefore be determined numerically by finding the minimum of the total dissipation

$$D_{\text{T}} = D_{\text{AB}} + D_{\text{BC}} + D_{\text{B′B}} \tag{18}$$

with respect to the thrust dips θ and φ.

4. Inversion of dip data

The inverse problem is as follows: What are the values of the friction coefficients compatible with the observed dips of our 12 experiments? There are only three friction coefficients at stake: the friction angle of the sand on the imposed ramp α_{R}, and on the flat α_{F}, and the internal friction angle of the sand α_{B}. The friction on the flat α_{F} appears only in case 3 (Fig. 4) and has a very small effect on the optimal thrust dips (Maillot and Leroy, 2003). We therefore eliminate it from the inversion and set $\alpha_{\text{F}} = 23°$ in all the calculations, which corresponds to the material of the bottom of the box (fiber glass sheet). The parametric space of the inversion is thus reduced to two coefficients, α_{R} and α_{B}, and can be fully explored by numerical means.

Since four types of ramp materials were used (groups, A, B, C, and D in Table 1), the inversion must be carried out independently for each type to yield a friction coefficient α_{R} for each material. Also, since the same sand was used in all experiments, a single internal friction coefficient α_{B} is sought. The inversion consists in calculating a misfit between the observed and the theoretical thrust dips for every possible value of α_{R} and α_{B}. Since the experimental data follow a Gaussian distribution, we define the misfit with the L2 norm:

$$M_X(\alpha_{\text{R}}, \alpha_{\text{B}}) = \sum_{i=1}^{n_X} \left(\frac{\overline{\varphi}(i) - \varphi_{\text{opt}}(\alpha_{\text{R}}, \alpha_{\text{B}})}{\sigma_\varphi(i)}\right)^2$$
$$+ \left(\frac{\overline{\theta}(i) - \theta_{\text{opt}}(\alpha_{\text{R}}, \alpha_{\text{B}})}{\sigma_\theta(i)}\right)^2 \tag{19}$$

where X stands for the type of ramp material (A, B, C, or D), and n_X is the number of experiments with ramp material X. The probability, or likelihood, of the couple (α_{R}, α_{B}),

$$P_X(\alpha_{\text{R}}, \alpha_{\text{B}}) \propto e^{-\frac{1}{2}M_X(\alpha_{\text{R}}, \alpha_{\text{B}})}, \tag{20}$$

is shown in Fig. 6. For each type of ramp material, abscissae represent α_{R}, and ordinates α_{B}. For groups A, C, and D, the distributions exhibit the same important features: zero probabilities in the half-space $\alpha_{\text{R}} > \alpha_{\text{B}}$, and nearly constant probabilities in the direction $\alpha_{\text{R}} + \alpha_{\text{B}} = $ constant. The former is due to the absence of shortcuts (kinematic case 1) in groups A, C, and D (except for experiment number 9). It is, however, precisely because our forward modelling integrated the possibility of shortcuts that their actual absence is significant and leads to this very sharp drop of probability along the line
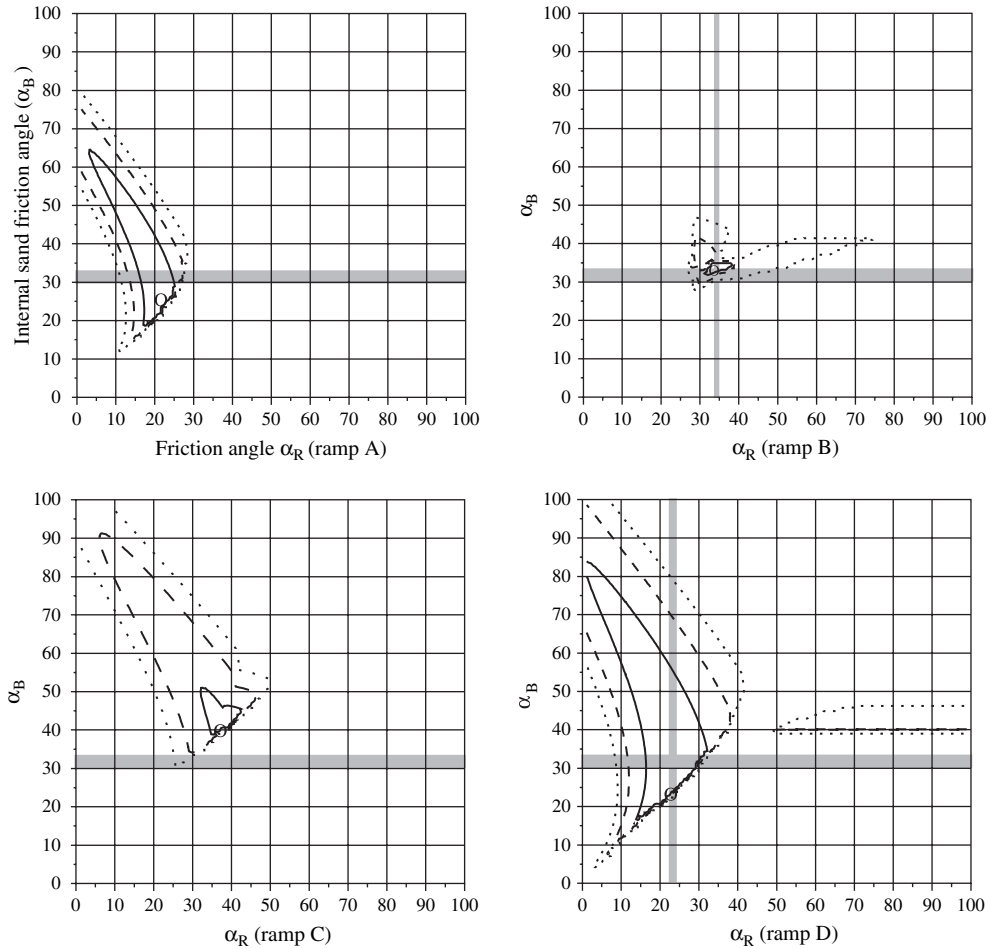
Fig. 6. Probability function (normalised by their maximum value) for each group of experiments. Abscissae: friction along the ramps A (top left), B (top right), C (bottom left), and D (bottom right). Ordinates: internal friction angle of the sand. Level curves are drawn at 5% (dotted), 20% (dashed), and 60% (solid). Grey bars indicate independent friction measurements.

$\alpha_R = \alpha_B$. The latter is due to the structure of the solution (13) for case 1 (Fig. 5) which is very sensitive to the sum $\alpha_R + \alpha_B$ and much less to the difference $\alpha_R - \alpha_B$. In contrast to the groups A, C and D, in group B the probability that $\alpha_R > \alpha_B$ is not zero because shortcuts appeared systematically, making the kinematic model in case 2 the most efficient, and implying that the difference $\alpha_R - \alpha_B$ remains small. The probability distribution appears very well focused, making the group B experiments the most informative as will be confirmed by the analysis of marginal probabilities. The grey bars indicate independent measurements of the friction angles (Maillot and Koyi, 2006) remembering that frictions on ramps A and C have not been measured. They are in very good agreement with the probability densities, except for group C. Here, we observe a discrepancy of about 10° between the probability distribution of α_B and its value measured independently (Fig. 6, bottom left, and Fig. 8). It is probably due to the fact that experiment 9 has the highest ramp dip of group C and was therefore expected to be very informative (like experiments 4, 5, and 12 for the groups A, B, and D, respectively). The change in kinematic scenario in experiment 9 (recall that it shifts from case 1 to case 3 along strike) results in an overestimation of the sand internal friction angle. Indeed, the analytical solution presented in Fig. 5 (solid curve) shows that a low thrust dip θ results from a high ramp friction α_R. Conversely, an underestimated ramp dip (because of the occurrence of case 3) will imply an overestimation of the thrust friction angle.

In support of the above interpretations in terms of qualitative variations in the kinematics, we show in Fig. 7 the probability distributions obtained when ignoring the possibility of shortcuts in the forward modelling (case 1 only is considered, and thus $\varphi_{opt} = \varphi'$). The nearly constant distributions in the direction $\alpha_R + \alpha_B = $ constant are preserved because they come from the solution of case 1. However, there is now no drop in probability for $\alpha_R \geq \alpha_B$. Very low and very high α_B are now probable, and the ramp frictions α_R are also less constrained. The distribution for the group B (top left) is completely different for obvious reasons (shortcuts occurred systematically). Thus, the comparison of Figs. 6 and 7 show that substantial information can be extracted if one includes different kinematic scenarios in the forward modelling. It is not even necessary that these kinematics have been observed: they only need to be possible within the investigated range of parameters.
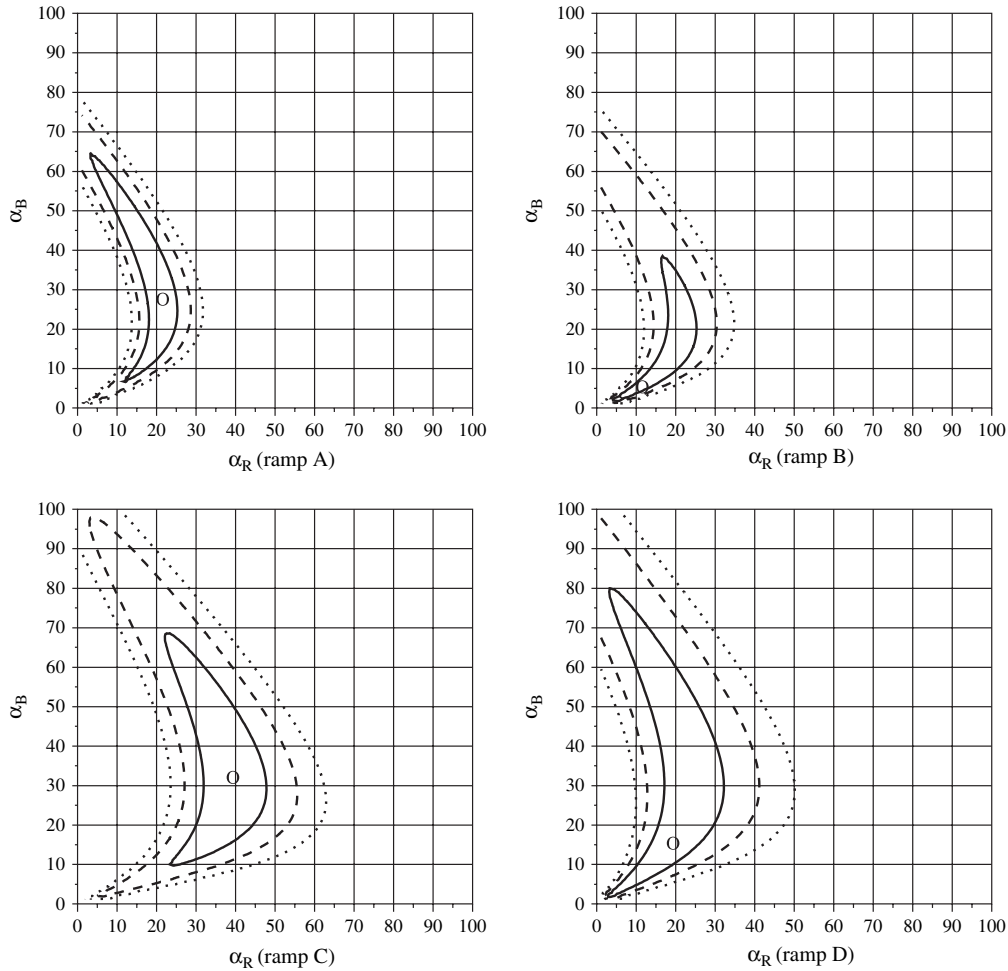
Fig. 7. Same caption as Fig. 6. Here, the probability functions are evaluated by considering only the kinematic case 1 in the forward modelling, ignoring the possibility of shortcuts (cases 2 and 3).

Exact equality in Eq. (20) is obtained by normalising the right hand side by its total integral (α_R and α_B ranging over $[0°, 90°]$). Then, marginal probabilities can be computed to obtain the likelihood of each parameter independently of the other ones. Starting with the internal sand friction, α_B, the marginal probabilities for each group of experiments,

$$P_X(\alpha_B) = \int_0^{\pi/2} P_X(\alpha_R, \alpha_B)\, d\alpha_R, \qquad (21)$$

are shown in Fig. 8 where X stands for A, B, C or D. Clearly, the experiments of group B give the best information on α_R, in very close agreement with the independent measurements (grey bar). The other groups of experiments are much less constraining on α_B. The total probability considering all 12 experiments,

$$P(\alpha_B) = (4P_A(\alpha_B) + 2P_B(\alpha_B) + 3P_C(\alpha_B) + 3P_D(\alpha_B))/12, \qquad (22)$$

is illustrated in Fig. 8 by a thick solid line and exhibits the two peaks, respectively, due to experiments A, B, and C, D.
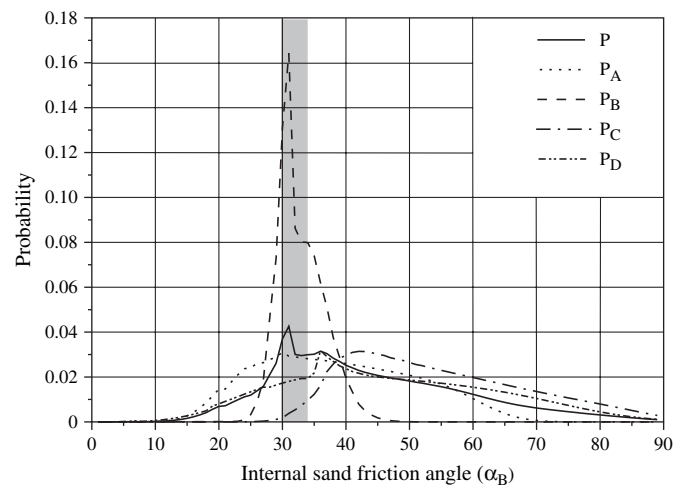

Fig. 8. Probability of internal friction angle of the sand for each group of experiments (21). Curves as indicated. The solid curve is the mean probability weighted by the number of experiments in each group (22). The grey bar indicates independent friction measurements.
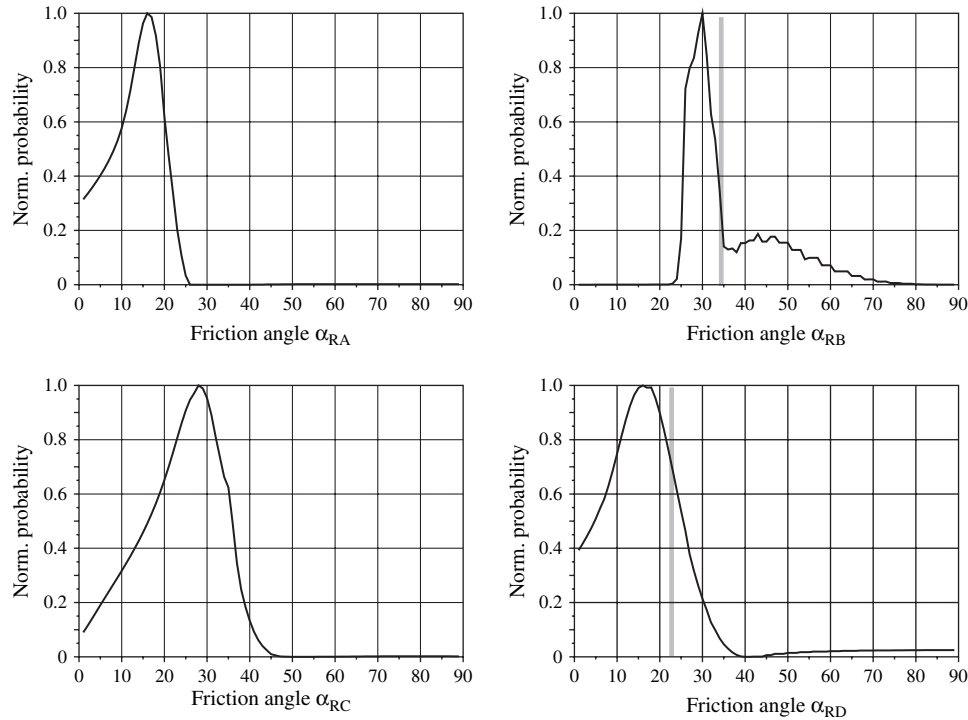
Fig. 9. Normalised probability of ramp friction angle for each group of experiments. Ramps A (top left), B (top right), C (bottom left), and D (bottom right). Grey bars in B and D indicate independent friction measurements.

Similarly, the marginal probabilities for α_R are illustrated in Fig. 9. For groups A, C, and D, the distributions give upper bounds for α_R (respectively, 25°, 45°, and 35°) because, again, no shortcut appeared for all ramp dips tested. For group B, the distribution gives 23° as a lower bound for α_R. The sharpness of the probability function is significant, and indicates a relative order of the ramp friction values as ramp A < ramp D < ramp C < ramp B, in agreement with the available independent measurements.

5. Conclusion

The set of 12 experiments presented here involves a very simple horizontal shortening of a homogeneous sand layer over an imposed rigid ramp with varying dips and friction coefficients. We measured the dips of the thrusts occurring in the sand as it was forced to climb up the ramp. In certain combinations of ramp dip and ramp friction, the imposed ramp is shortcut by a less steep spontaneous ramp in the sand, and this was also measured. A χ^2 test allowed us to conclude that our data follow Gaussian distributions although some departures from that statistical model may be attributed to (i) lack of independent measurements (i.e., number of thrust segments that can be identified), (ii) systematic curvature of thrusts towards the ramp or surface, (iii) effects of finite box size, or sand heterogeneity. Effects of layer thickness and total amount of shortening, pre-compaction, dilatancy, fault curvature, along strike variations, are all seen as second order features which are not taken into account in the forward modelling of the dip data. All these parameters potentially

contribute to increase the standard deviations and thus render the experiments less informative. Quantitative interpretations of these observations were carried out by an inversion procedure using the L2 norm between observed and predicted ramp and thrust dips.

The theory used to model these data is based on the geometrical description of the thrusts from which mean forces are evaluated by invoking global force balance. Forces and slip velocities along the faults were then combined to compute the dissipation of mechanical work. Thrust dips are predicted by minimising the total dissipation with respect to ramp and thrust dips. This exercise was repeated for three kinematic scenarios (no shortcut, steeper shortcut, less steep shortcut). The predicted scenario is the one that yields the least total dissipation. Analytical solutions are given for the first two cases.

The inversion presented here aims to evaluate the probability distributions of five friction coefficients: that of the sand, and one for each of the four ramp materials used. Internal sand friction is best constrained because all 12 experiments help to constrain its value. The sharp peak in its distribution coincides exactly with independent measurements of the friction. However, a very large range of values (25−65°) have non-negligible probabilities, thus reflecting experimental imperfections as well as the highly variable character of the friction coefficient, known to be difficult to reproduce experimentally. More interestingly perhaps are the results on the ramp frictions. For groups A and B, they show sharp transitions that provide bounds that are not obvious ($\alpha_{RA} < 25°$ $< \alpha_{RB} \leq 35°$). These transitions are due to the occurrence of shortcuts which is a qualitative, easily measured, effect that

is the result of small changes in continuous variables such as the friction coefficient. Thus, because the dips are very smooth functions of the ramp friction coefficients, their sole measurement does not constrain the friction parameters very well. One must additionally study global changes in the geometry (dips) of the thrusts: it is the very fact that a geometry is *possible*, or *not possible*, that is very informative.

Acknowledgements

References

Bonini, M., Sokoutis, D., Mulugeta, G., Katrivanos, E., 2000. Modelling hanging wall accommodation above rigid thrust ramps. Journal of Structural Geology 22, 1165−1179.

Buiter, S.J.H., Babeyko, A.Y., Ellis, S., Gerya, T.V., Kaus, B.J.P., Kellner, A., Schreurs, G., Yamada, Y., 2006. The numerical sandbox: comparison of model results for a shortening and an extension experiment. In: Buiter, S.J.H., Schreurs, G. (Eds.), Analogue and Numerical Modelling of Crustal-Scale Processes. Geological Society, London, Special Publications, vol. 253, pp. 29−64.

Colletta, B., 2005. Passive and active inherited faults in fold and thrust belts. In: Keynote Abstract in Thrust Belts and Foreland Basins International Meeting, Reuil-Malmaison, France.

Erickson, J.P., Jamison, W.R., 1995. Viscous-plastic finite element models of fault-bend folds. Journal of Structural Geology 17 (4), 561−573.

Erickson, J.P., Strayer, L.M., Suppe, J., 2001. Initiation and reactivation of faults during movement over a thrust-fault ramp: numerical mechanical models. Journal of Structural Geology 23, 11−23.

Grelaud, S., Buil, D., Hardy, S., Frizon de Lamotte, D., 2000. Trishear kinematic model of fault-propagation folding and sequential development of minor structures: the Oupia anticline (NE Pyrenées, France) case study. Bulletin de la Société Géologique de France 171, 441−449.

Lohrmann, J., Kukowski, N., Adam, J., Oncken, O., 2003. The impact of analogue material properties on the geometry, kinematics, and dynamics of convergent sand wedges. Journal of Structural Geology 25, 1691−1711.

Maillot, B., Leroy, Y.M., 2003. Optimal dip based on dissipation of back thrusts and hinges in fold-and-thrust belts. Journal of Geophysical Research 108 (B6), 2320−2339.

Maillot, B., Koyi, H., 2006. Thrust dip and thrust refraction in fault-bend-folds: analogue models and theoretical predictions. Journal of Structural Geology 28, 36−49.

Merchant, E., 1944. Basic mechanics of the metal cutting process. Journal of Applied Mechanics, 168−175.

Merle, O., Abidi, N., 1995. Approche expérimentale du fonctionnement des rampes émergentes. Bulletin de la Société Géologique de France 166 (5), 439−450.

Persson, K.S., 2001. Effective indenters and the development of double-vergent orogens: insights from analogue sand models. In: Koyi, H.A., Mancktelow, N.S. (Eds.), Tectonic Modelling: A Volume in Honor of Hans Ramberg. Geological Society of America Memoir 193, 191−206.

Rich, J.L., 1934. Mechanics of low-angle overthrust faulting as illustrated by Cumberland thrust block, Virginia, Kentucky, and Tennessee. Bulletin of the American Association of Petroleum Geologists 18 (12), 1584−1596.

Roure, F., Colletta, B., 1996. Cenozoic inversion structures in the foreland of the Pyrenées and Alps. In: Ziegler, P.A., Horvàth, F. (Eds.), Peri-Tethys Memoir 2: Structure and Prospects of Alpine Basins and Forelands. Mémoires du Museum National d'Histoire Naturelle 170, 173−209.

Schreurs, G., Buiter, S.J.H., Boutelier, D., Corti, G., Costa, E., Cruden, A., Daniel, J.-M., Hoth, S., Koyi, H., Kukowski, N., Lohrmann, J., Ravaglia, A., Schlische, R.W., Withjack, M.O., Yamada, Y., Cavozzi, C., DelVentisette, C., Elder Brady, J., Hoffmann-Rothe, A., Mengus, J.-M., Montanari, D., Nilforoushan, F., 2006. Analogue benchmarks of shortening and extension experiments. In: Buiter, S.J.H., Schreurs, G. (Eds.), Analogue and Numerical Modelling of Crustal-Scale Processes. Geological Society, London, Special Publications vol. 253, pp. 1−27.

Suppe, J., 1983. Geometry and kinematics of fault-bend folding. American Journal of Science 283 (7), 684−721.

Tarantola, A., 1987. Inverse Problem Theory. Elsevier, Amsterdam.

Turcotte, D.L., Schubert, G., 1982. Geodynamics, Applications of Continuum Physics to Geological Problems. John Wiley and Sons, New York.